

Minimal model for pulsar glitches

Neutron-superfluid vortices and
proton-superconductor flux tubes

This work is part of the PhD of 2 of **Rahul Pandit**'s students in IISc Bangalore:

Sanjay Shukla and **Akhilesh Kumar Verma**



Marc Brachet, LPENS

Rouen

23/9/2024

Conf 4 (14:00-14:40)



Talk outline I

Talk is about 4 publications with R. Pandit's Bangalore group

- Formation of compact objects at finite temperatures in a dark-matter-candidate self-gravitating bosonic system, PHYSICAL REVIEW RESEARCH 3, L022016 (2021)
- Rotating self-gravitating Bose-Einstein condensates with a crust: A model for pulsar glitches, PHYSICAL REVIEW RESEARCH 4, 013026 (2022)
- Gravity- and temperature-driven phase transitions in a model for collapsed axionic condensates, PHYSICAL REVIEW D 109, 063009 (2024)
- Neutron-superfluid vortices and proton-superconductor flux tubes: Development of a minimal model for pulsar glitches, arXiv:2405.12127, 2024

Talk outline II

Talk is about Self gravitating Bose Einstein Candidates

- Gross-Pitaevskii Equation with Newtonian gravitational potential generated by the BEC density
- With rotation
- With finite temperature modelled by classical field
- Also (in some cases) there is (beside the superfluid) a superconductor with magnetic field
- Obviously in 40 minutes I won't have time to go into details of 4 publications
- I'll try to give a view of the main physical ingredients and results

Talk outline III

Physical interest Self gravitating Bose Einstein Candidates

- Can describe bosons stars: gravitational collapse, steady states, rotation, finite temperature effects, phase transitions
- With rotation AND a crust: a model for pulsar glitches
- Adding a superconductor: a more 'realistic' model of pulsar glitches
- **In what follows:**
 - 1: Physical motivations
 - 2: Equations
 - 3: summary of results

Physical motivations I

Basic gravitating BEC

- In the GPE there is a condensate density field and a confining potential
- Idea: use the Newtonian gravity to confine the BEC

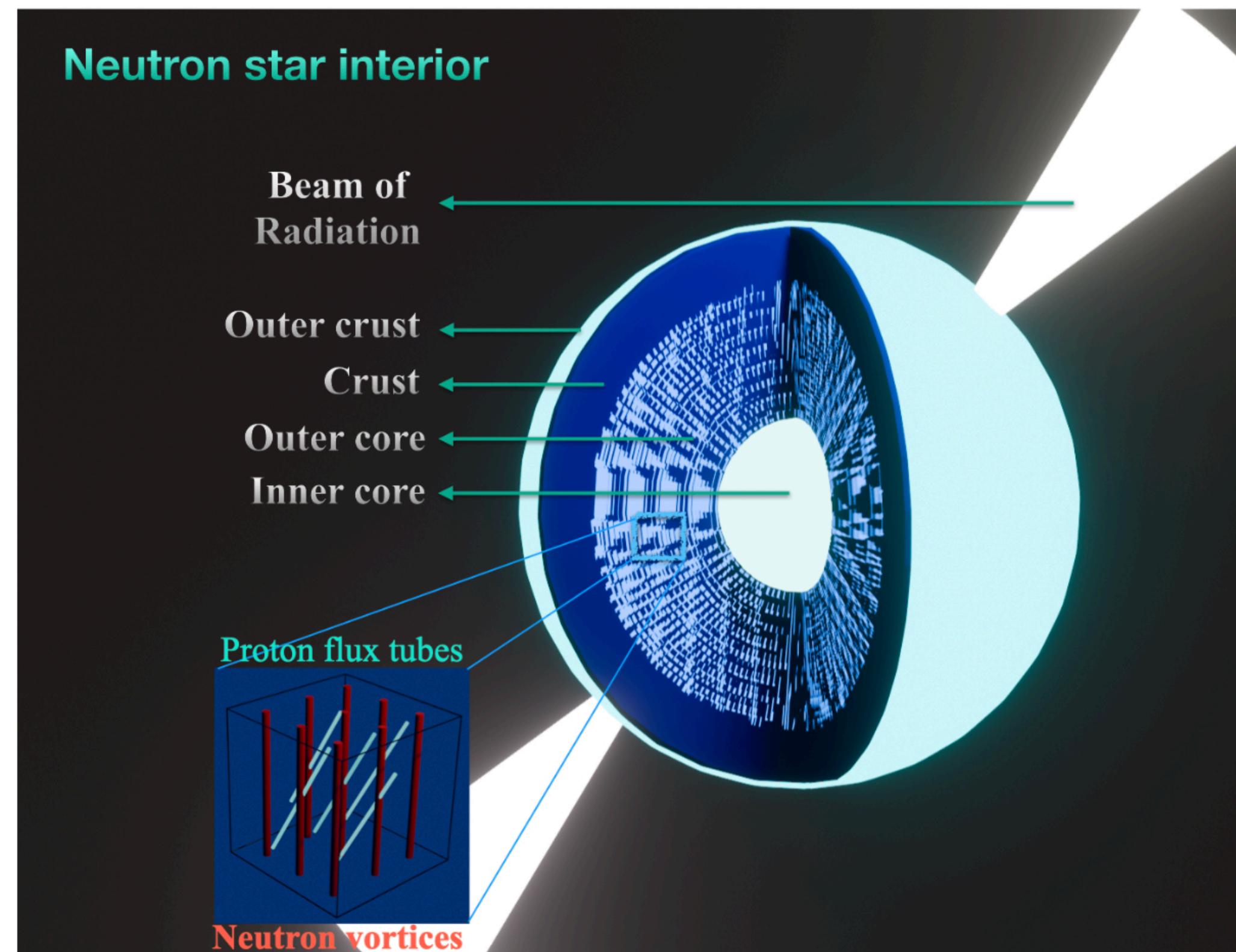
$$\begin{aligned} i\hbar\partial_t\psi &= -\frac{\hbar^2}{2m}\nabla^2\psi + [G\Phi + g|\psi|^2]\psi, \\ \nabla^2\Phi &= |\psi|^2 - \langle|\psi|^2\rangle, \end{aligned} \tag{1}$$

where m is the mass of the bosons, $n = |\psi|^2$ their number density, Φ is the gravitational potential field, $G = 4\pi G_N m^2$ (G_N is Newton's constant), and $g = 4\pi a\hbar^2/m$, with a the

Physical motivations II

Astrophysical 'objects'

- Boson stars
- Self-gravitating dark matter: 'axions' halos
- Pulsars/neutron stars : BEC of cooper pairs of neutron and proton



Self-gravitating bosonic system

Boson star, no rotation

function}, the Fourier-truncated GPPE becomes

$$i\hbar \frac{\partial \psi}{\partial t} = \mathcal{P}_G \left\{ -\frac{\hbar^2}{2m} \nabla^2 \psi + \mathcal{P}_G[(G\nabla^{-2} + g)|\psi|^2]\psi \right\}. \quad (2)$$

directly by using the SGLPE,

$$\begin{aligned} \hbar \frac{\partial \psi}{\partial t} = \mathcal{P}_G \left\{ \frac{\hbar^2}{2m} \nabla^2 \psi + \mu \psi - \mathcal{P}_G[(G\nabla^{-2} + g)|\psi|^2]\psi \right\} \\ + \sqrt{\frac{2\hbar}{\beta}} \mathcal{P}_G[\zeta(\mathbf{x}, t)], \end{aligned} \quad (3)$$

where the zero-mean, Gaussian white noise $\zeta(\mathbf{x}, t)$ has the variance $\langle \zeta(\mathbf{x}, t) \zeta^*(\mathbf{x}', t') \rangle = \delta(t - t') \delta(\mathbf{x} - \mathbf{x}')$, with $\beta =$

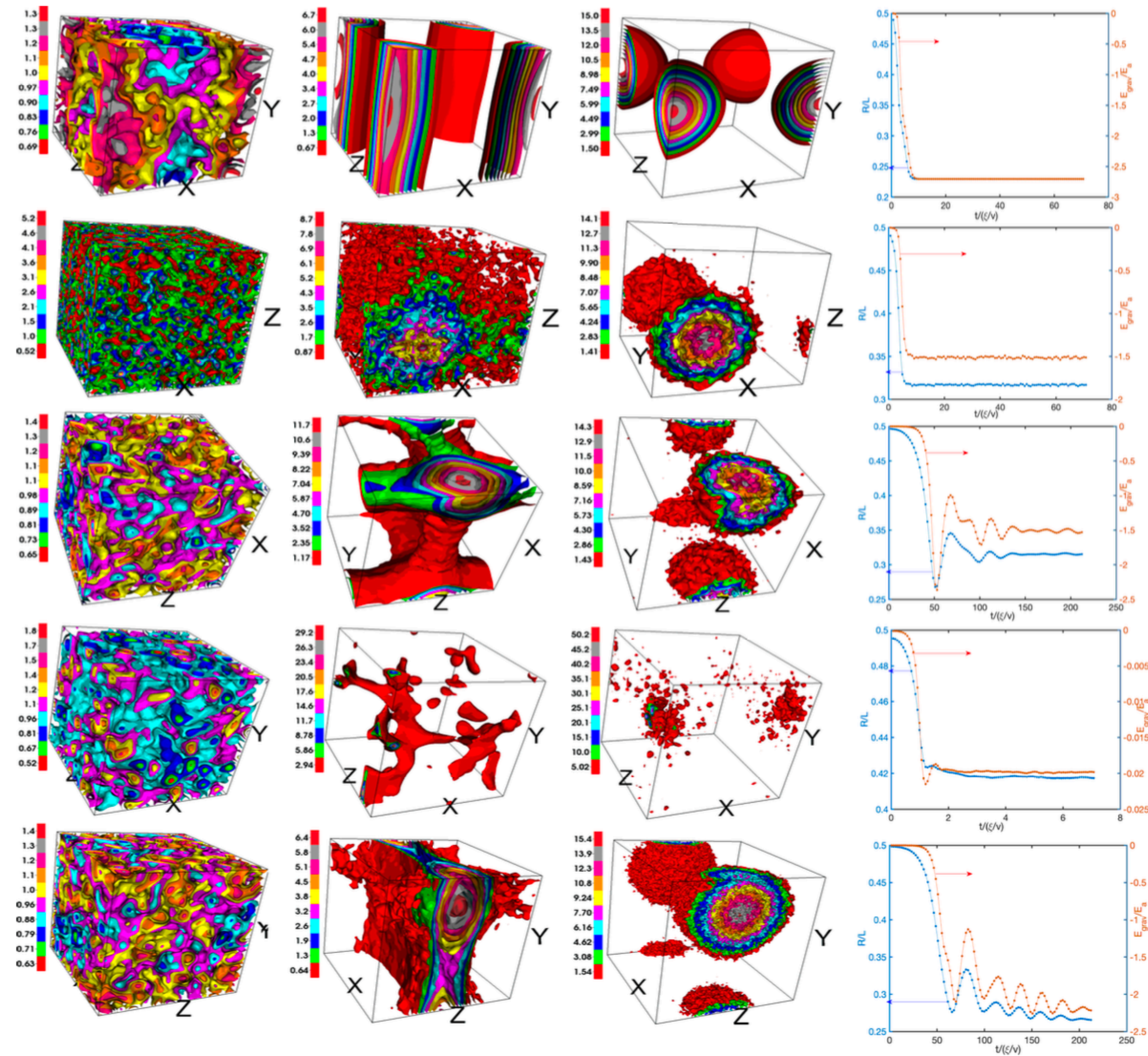


FIG. 1. Columns 1–3 show 10-level contour plots of $|\psi(\mathbf{x}, t)|^2$ at representative times: SGLPE ($T = 0$) (top row, run R1), SGLPE (second row, run R2), GPPE (third row, run R3), GPPE (fourth row, run R4), and 256^3 GPPE (fifth row, run R5; Supplemental Videos S1–S5 in the Supplemental Material [22] show, respectively, the complete spatiotemporal evolution for these cases). Column 4: Plots of the scaled radius of gyration $\frac{R}{L} = \frac{1}{L} \sqrt{\frac{\int_V \rho(r) r^2 d\mathbf{x}}{\int_V \rho(r) d\mathbf{x}}}$ (blue) and the scaled gravitational energy E_{grav}/E_a (red) versus the scaled time $t/(\xi/v)$ for the different runs, where $E_a = 2^5 \pi^4 (G/g^3)^{1/2}$.

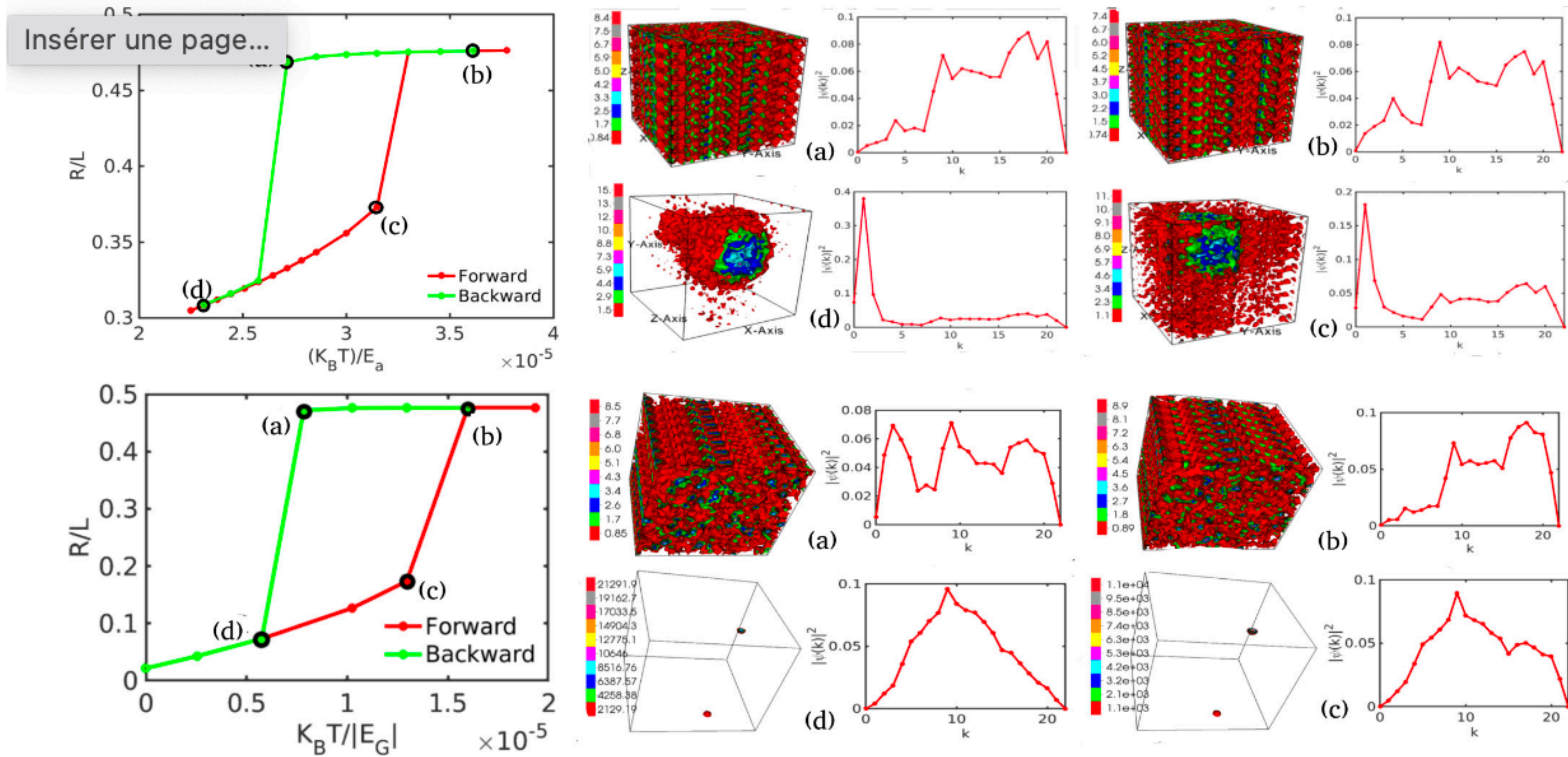


FIG. 3. Top left panel: plots of the dimensionless radius (R/L) versus the dimensionless temperature ($k_B T/E_a$), for heating (red) and cooling (green) runs showing a hysteresis loop. We show 10-level contour plots of $|\psi(\mathbf{x})|^2$ and the associated spectra $|\psi(k)|^2$ to illustrate, at representative points on heating and cooling curves in the hysteresis plot, the real-space density distribution and the k -space density spectra [$k_B T/E_a = 2.7 \times 10^{-5}$ and $k_B T/E_a = 3.62 \times 10^{-5}$ in (a) and (b) of the top panels, respectively, and $k_B T/E_a = 2.3 \times 10^{-5}$ and $k_B T/E_a = 3.16 \times 10^{-5}$ in (c) and (d) of the bottom panels, respectively]. The analogs of these plots, for the case $g = 0$, are shown in the panels at the very bottom. In the bottom left panel we use $|E_G|$ at $T = 0$ to make the temperature dimensionless.

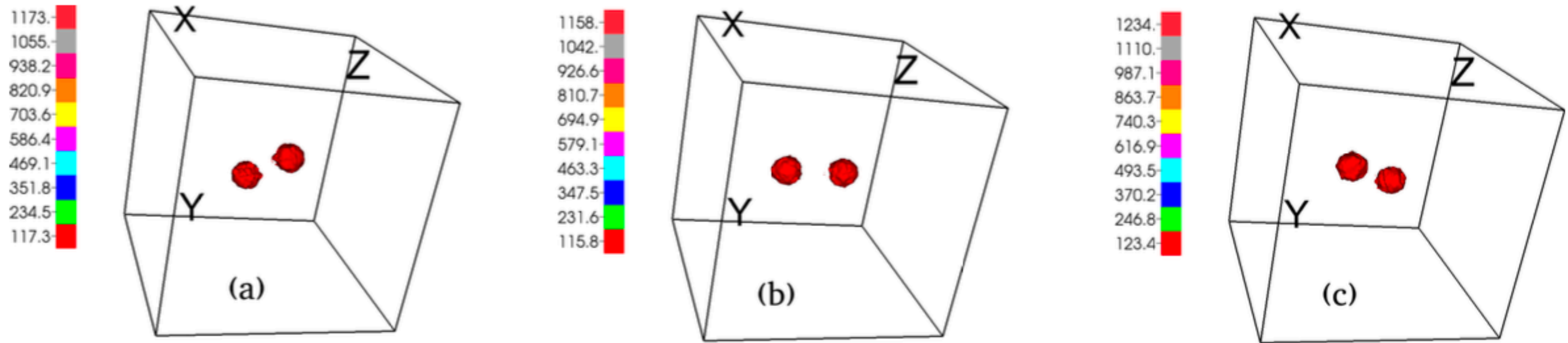


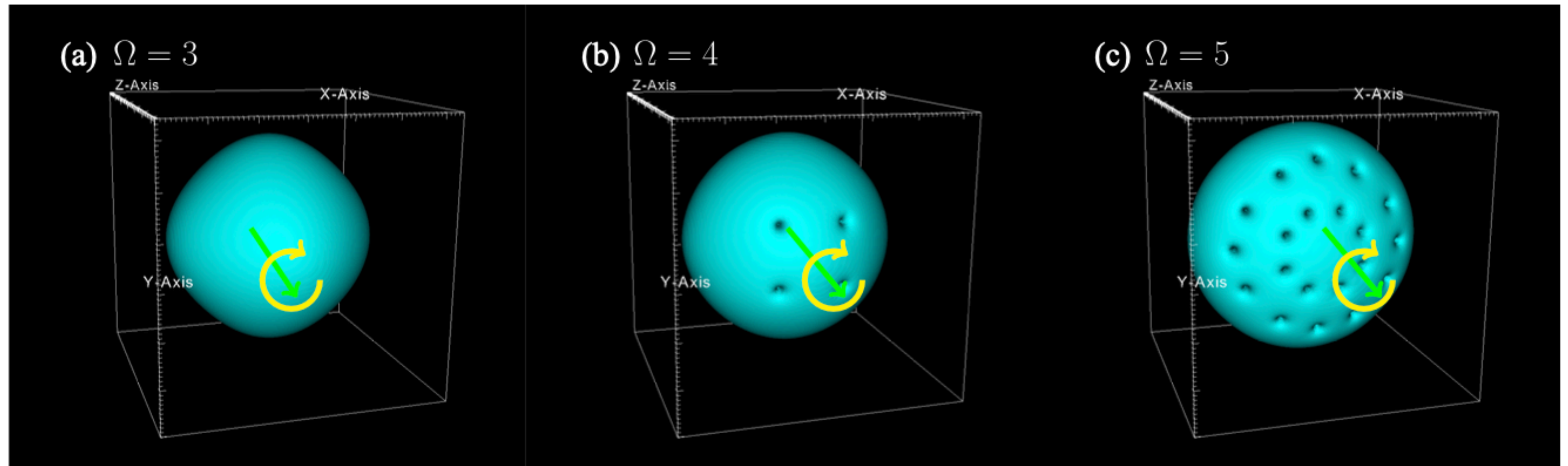
FIG. 4. Ten-level contour plots of the $|\psi(\mathbf{x}, t)|^2$ (a) at $t = 0.018$, (b) at $t = 0.025$, and (c) at $t = 0.03$, for the initial condition for $\psi(\mathbf{x}, t)$ given in Eq. (1) of the Supplemental Material [22], showing the rotating binary system (see Supplemental Video S6 in the Supplemental Material).

Rotating self-gravitating Bose-Einstein condensates

a model for collapsed axionic condensates

$$i\hbar \frac{\partial \psi}{\partial t} = -\frac{\hbar^2}{2m} \nabla^2 \psi + [G\Phi + g|\psi|^2 + g_2|\psi|^4]\psi,$$
$$\nabla^2 \Phi = |\psi|^2 - \langle |\psi|^2 \rangle,$$

$$\hbar \frac{\partial \psi}{\partial t} = \frac{\hbar^2}{2m} \nabla^2 \psi - [G\Phi + g|\psi|^2 + g_2|\psi|^4 - \Omega L_z]\psi.$$



Rotating self-gravitating Bose-Einstein condensates with a crust: A model for pulsar glitches

introducing the crust

scattering length [29]. We describe the dynamics of the pulsar's solid crust by a single polar angle θ , which evolves as follows:

$$i\hbar\partial_t\psi = -\frac{\hbar^2}{2m}\nabla^2\psi + [V_\theta + G\Phi + g|\psi|^2]\psi, \quad (1)$$

$$\nabla^2\Phi = |\psi|^2 - \langle|\psi|^2\rangle. \quad (2)$$

$$I_c \frac{d^2\theta}{dt^2} = \frac{1}{N} \int d^3x \partial_\theta V_\theta |\psi|^2 - \alpha \frac{d\theta}{dt}, \quad (3)$$

$$V_\theta(\mathbf{r}_p) = V_0 \exp\left(-\frac{|\mathbf{r}_p| - r_{\text{crust}}}{\Delta r_{\text{crust}}}\right)^2 \tilde{V}(x_\theta, y_\theta). \quad (4)$$

I_c and V_θ denote the moment of inertia of the crust and the crust potential, respectively; α controls the frictional slowing down of the rotation of the crust, with $\sqrt{I_c/\alpha}$ being the crust-friction decay time; for specificity, we choose $\tilde{V}(x_\theta, y_\theta) = 3 + \cos(n_{\text{crust}}x_\theta) + \cos(n_{\text{crust}}y_\theta)$, with $x_\theta = \cos(\theta)x_p + \sin(\theta)y_p$ and $y_\theta = -\sin(\theta)x_p + \cos(\theta)y_p$;

We first obtain uniformly rotating states for the GPPE with rotational speed Ω by solving the imaginary-time equation

$$\hbar\partial_t\psi = -\frac{\delta}{\delta\bar{\psi}}\left(E - \Omega J_z - \mu N - \lambda\left(\frac{\mathbf{P}}{N_0 m}\right)^2\right). \quad (6)$$

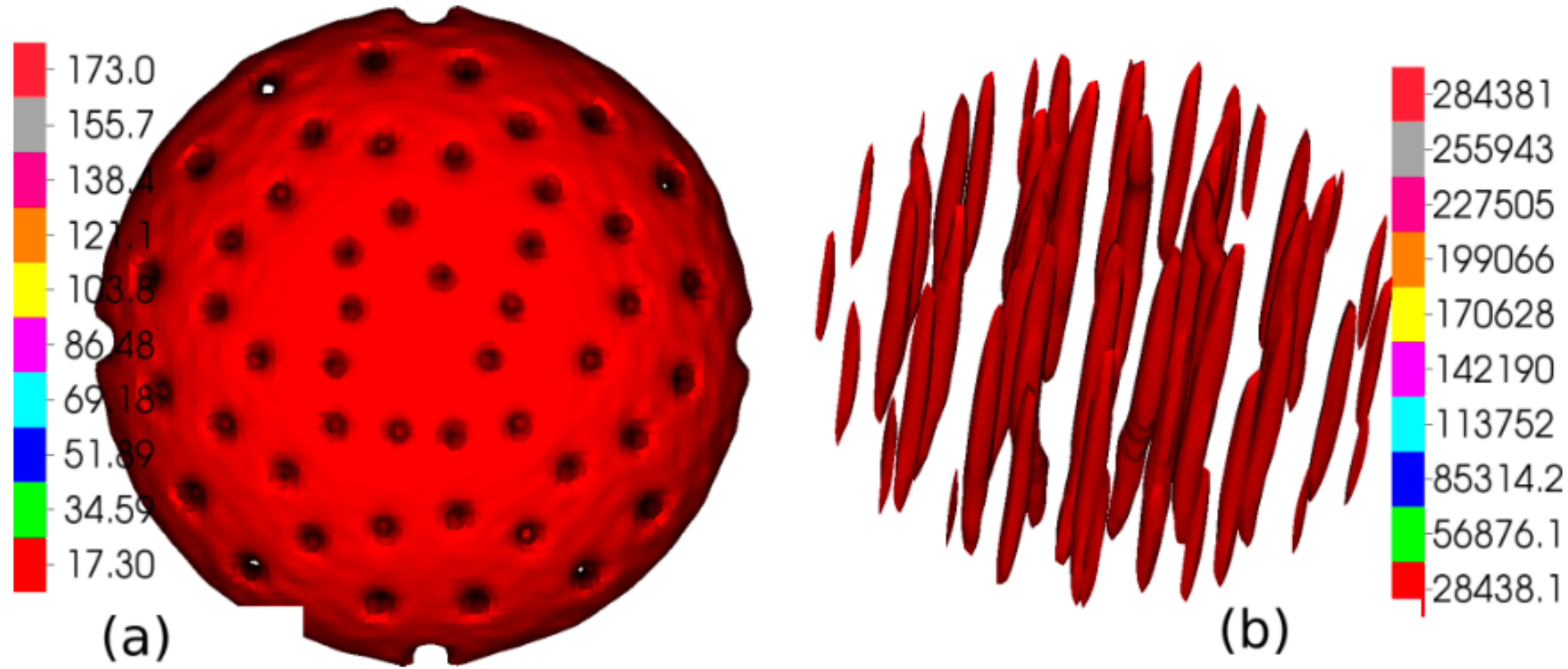


FIG. 2. Isosurface plots illustrating a rotating, compact object with vortices obtained via the ARGLPE (see text): (a) Isosurfaces of the boson density (top view) (for the spatiotemporal evolution of these isosurfaces, see Video S1 in the Supplemental Material [34]) and (b) isosurfaces of $(\nabla \times (\rho v))^2$ (side view); here, $\mathcal{N} = 256$, $G = 800$, $g = 80$, and $\Omega = 60$.

Then we use the preparation

$$\begin{aligned} \hbar \frac{\partial \psi}{\partial t} = & \frac{\hbar^2}{2m} \nabla^2 \psi + \mu \psi - [V_\theta + (G \nabla^{-2} + g) |\psi|^2] \psi \\ & - i \hbar \left(\Omega \hat{\mathbf{e}}_z \times \mathbf{r}_p - \lambda \frac{\mathbf{P}}{N_0 m} \right) \cdot \nabla \psi, \end{aligned} \quad (7)$$

which we solve to obtain the rotational ground states (minima) mentioned above; to stabilize this minimization procedure, we reset the center of mass $\mathbf{r}_{cm} = \int d^3x \mathbf{r}_p |\psi|^2 / N$ to $(\pi, \pi, 0)$, after each time step.

then we solve the BEC/crust GPPE coupled equations

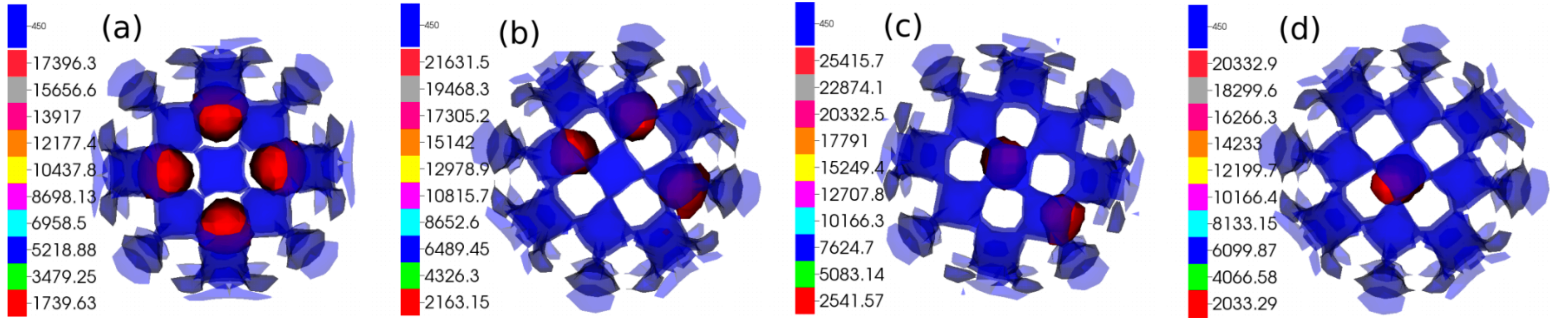


FIG. 3. Plots of crust-potential isosurfaces in blue, with $V_\theta = 450$, and of ten-level isosurfaces of $(\nabla \times (\rho v))^2$, from our DNS of the GPPE, for the representative parameter values $V_0 = 180$, $n_{\text{crust}} = 12$, $I_c = 0.01$, $r_{\text{crust}} = 1.0$, $\Delta r_{\text{crust}} = 0.15$, $\Omega_0 = 14$, and $\alpha = 0.007$ (as in Fig. 4 below) at times (a) $t = 0.06$, (b) $t = 6.48$, (c) $t = 7.38$, and (d) $t = 9.72$. For the spatiotemporal evolution of these isosurfaces, see Video S2 in the Supplemental Material [34].

This procedure generates vortex slips and glitches

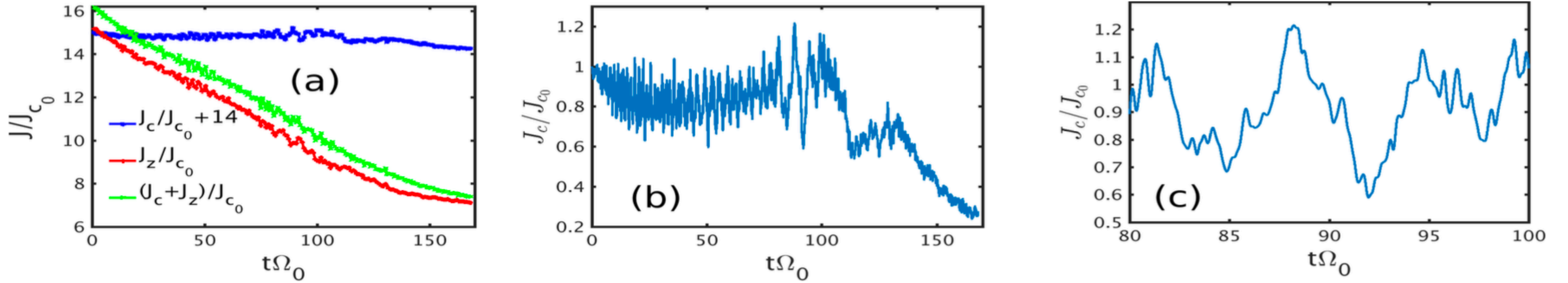


FIG. 4. (a) Plots, vs the scaled time $t\Omega_0$, of $(J_c/J_{c_0} + 14)$ (blue curve), J_z/J_{c_0} (red curve), and $(J_c + J_z)/J_{c_0}$ (green curve), where J_{c_0} is the initial angular momentum of the crust, for the representative parameter values given in Fig. 3 above. Expanded plots of J_c/J_{c_0} for (b) $0 < t\Omega_0 \lesssim 170$ and (c) $80 \leq t\Omega_0 \leq 100$.

SOC Glitch data analysis

Power laws in CDF of gain of crust angular momentum

we calculate the gain ΔJ_c in the crust angular momentum, between successive minima and maxima of $J_c(t)$; we call ΔJ_c the event size; we scale it by J_{c_0} . In Fig. 5(a) we present a log-log (base 10) plot of the cumulative probability distribution function (CPDF) $Q(\Delta J_c/J_{c_0})$; this yields the power-law behavior $Q(\Delta J_c/J_{c_0}) \sim (\Delta J_c/J_{c_0})^\beta$ for the part of the CPDF that lies in the region shaded gray. Thus the probability distribution function (PDF) $P(\Delta J_c/J_{c_0}) \sim (\Delta J_c/J_{c_0})^{\beta-1}$; by fitting the CPDF in the gray region, we find $\beta \simeq 0.7 \pm 0.1$.

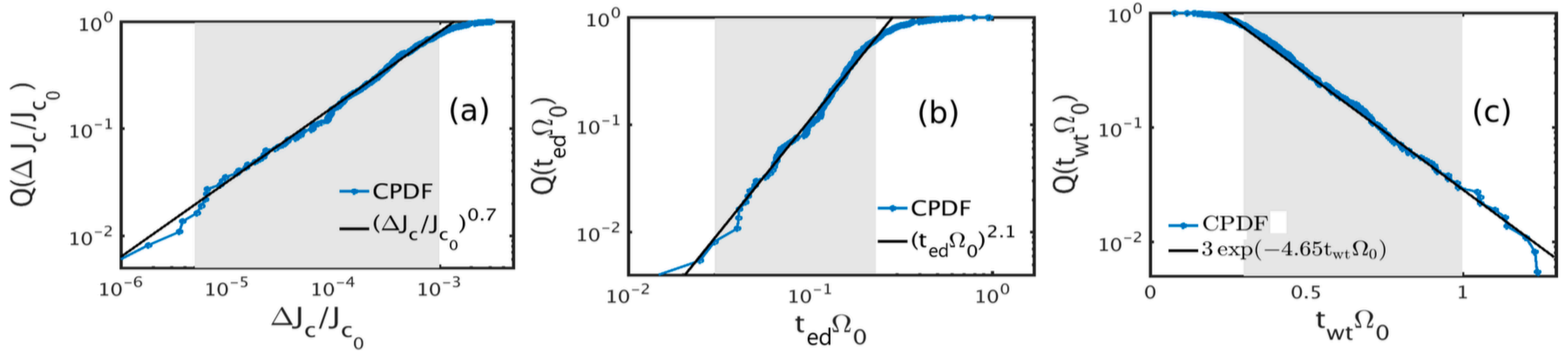


FIG. 5. Log-log (base 10) plots of (a) the CPDF $Q(\Delta J_c/J_{c_0})$ of the event size and (b) the CPDF $Q(t_{ed}\Omega_0)$ of the event duration. (c) Semilog (base 10) plot of the CPDF $Q(t_{wt}\Omega_0)$. J_{c_0} and Ω_0 are the initial angular momentum and angular velocity of the crust, respectively. Our DNS data are shown in blue; the black lines show fits (power law or exponential) to these data in the shaded gray regions in the plots.

Previous papers show that the power-law exponent of the glitch size has the following values: 0.02 with moat and 0.81 without moat in Ref. [38], between 1 and 2 in Ref. [39], and 1.31 in Ref. [40]. Previous papers such as Refs. [38–40] focus on the sizes and waiting times of the events, but not their durations, which are an element in this paper. Indeed, our work should be relevant to new investigations in which glitch durations are being resolved well [41–43].

Neutron-superfluid vortices and proton-superconductor flux tubes

Development of a minimal model for pulsar glitches

$$\begin{aligned} \mathcal{L}_n = & \frac{i\hbar}{2} \left(\psi_n^* \frac{\partial \psi_n}{\partial t} - \psi_n \frac{\partial \psi_n^*}{\partial t} \right) - \frac{\hbar^2}{2m_n} |\nabla \psi_n|^2 \\ & - \frac{g}{2} \left(|\psi_n|^2 - \frac{\mu_n}{g} \right)^2 - m_n \Phi |\psi_n|^2 - \frac{1}{8\pi G} (\nabla \Phi)^2 \\ & - V_\theta |\psi_n|^2 + \frac{i\hbar}{2} (\boldsymbol{\Omega} \times \mathbf{r}) \cdot (\psi_n \nabla \psi_n^* - \psi_n^* \nabla \psi_n), \quad (1) \end{aligned}$$

$$\begin{aligned} \mathcal{L}_p = & \frac{i\hbar}{2} \left(\psi_p^* \frac{\partial \psi_p}{\partial t} - \psi_p \frac{\partial \psi_p^*}{\partial t} \right) - \frac{1}{2m_p} |D_{\mathbf{A}} \psi_p|^2 \\ & - \frac{\alpha_s}{2} \left(|\psi_p|^2 - \frac{\mu_p}{\alpha_s} \right)^2 - q\phi |\psi_p|^2 - m_p \Phi |\psi_p|^2 - V_\theta |\psi_p|^2 \\ & + \frac{1}{2} (\boldsymbol{\Omega} \times \mathbf{r}) \cdot (\psi_p D_{\mathbf{A}} \psi_p^* + \psi_p^* D_{\mathbf{A}} \psi_p), \end{aligned}$$

$$\begin{aligned} \mathcal{L}_{\text{EM}} = & \epsilon_0 \left[-\frac{1}{2} [\mathbf{E}^2 - c^2 (\mathbf{B} - \mathbf{B}_{\text{ext}})^2] \right. \\ & \left. + \mathbf{E} \cdot \left(-\nabla \phi - \frac{\partial \mathbf{A}}{\partial t} \right) - c^2 (\mathbf{B} - \mathbf{B}_{\text{ext}}) \cdot (\nabla \times \mathbf{A}) \right], \quad (3) \end{aligned}$$

$$\begin{aligned} \mathcal{L}_{\text{np}} = & \gamma \left\{ g_{np} |\psi_n|^2 |\psi_p|^2 \right. \\ & \left. - \frac{\hbar}{4i} (\psi_n \nabla \psi_n^* - \psi_n^* \nabla \psi_n) \cdot [\psi_p D_{\mathbf{A}} \psi_p^* + \psi_p^* D_{\mathbf{A}} \psi_p] \right\} \end{aligned}$$

$$\begin{aligned} I_c \frac{d^2 \theta}{dt^2} = & \frac{1}{N_n} \left(\int d^3 x \partial_\theta V_\theta |\psi_n|^2 + \frac{n_n}{n_p} \int d^3 x \partial_\theta V_\theta |\psi_p|^2 \right) \\ & - \delta \frac{d\theta}{dt}; \\ V_\theta(\mathbf{r}_p) = & V_0 \exp \left[-\frac{(|\mathbf{r}_p| - r_{\text{crust}})^2}{(\Delta r_{\text{crust}})^2} \right] \tilde{V}(x_\theta, y_\theta); \end{aligned}$$

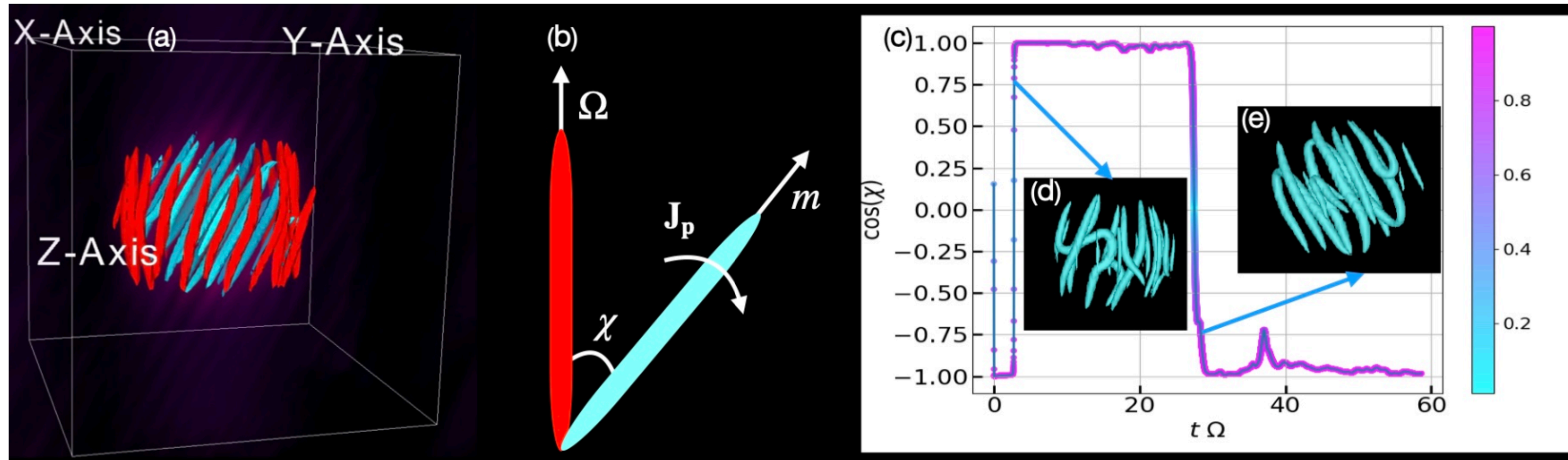
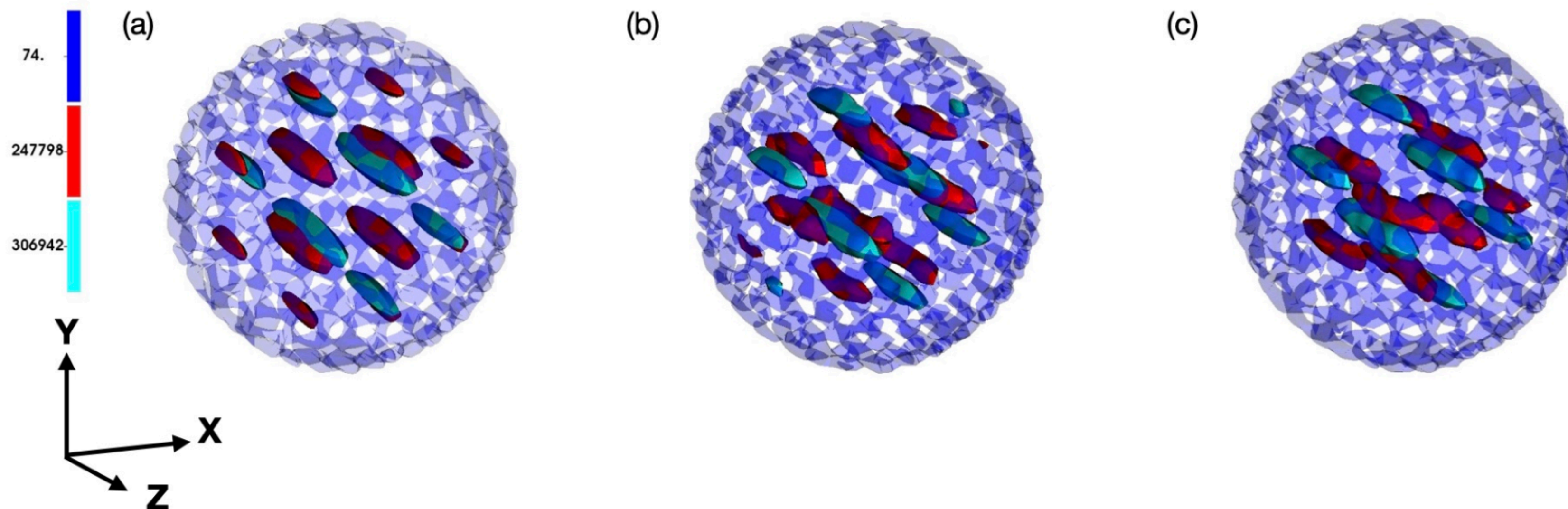


FIG. 11. Real-time evolution: **(a)** One-level contour plot of $(\nabla \times (\rho v))^2$ for neutron vortices (in red) and proton flux tubes (in cyan) at the initial time. **(b)** Schematic diagram showing the angle χ between the rotation axis and the magnetic moment [Eq. (40)]. **(c)** The evolution of the angle χ with time. Both neutron and proton subsystems rotate with angular velocity $\Omega = \Omega \hat{z}$, where $\Omega = 4.0$; and $B_{\text{ext}} = 0.8$, which makes an angle $\Theta = 30^\circ$ with the z -axis. Insets **(d)** and **(e)** show illustrative proton flux-tube configurations before and after the reversal.



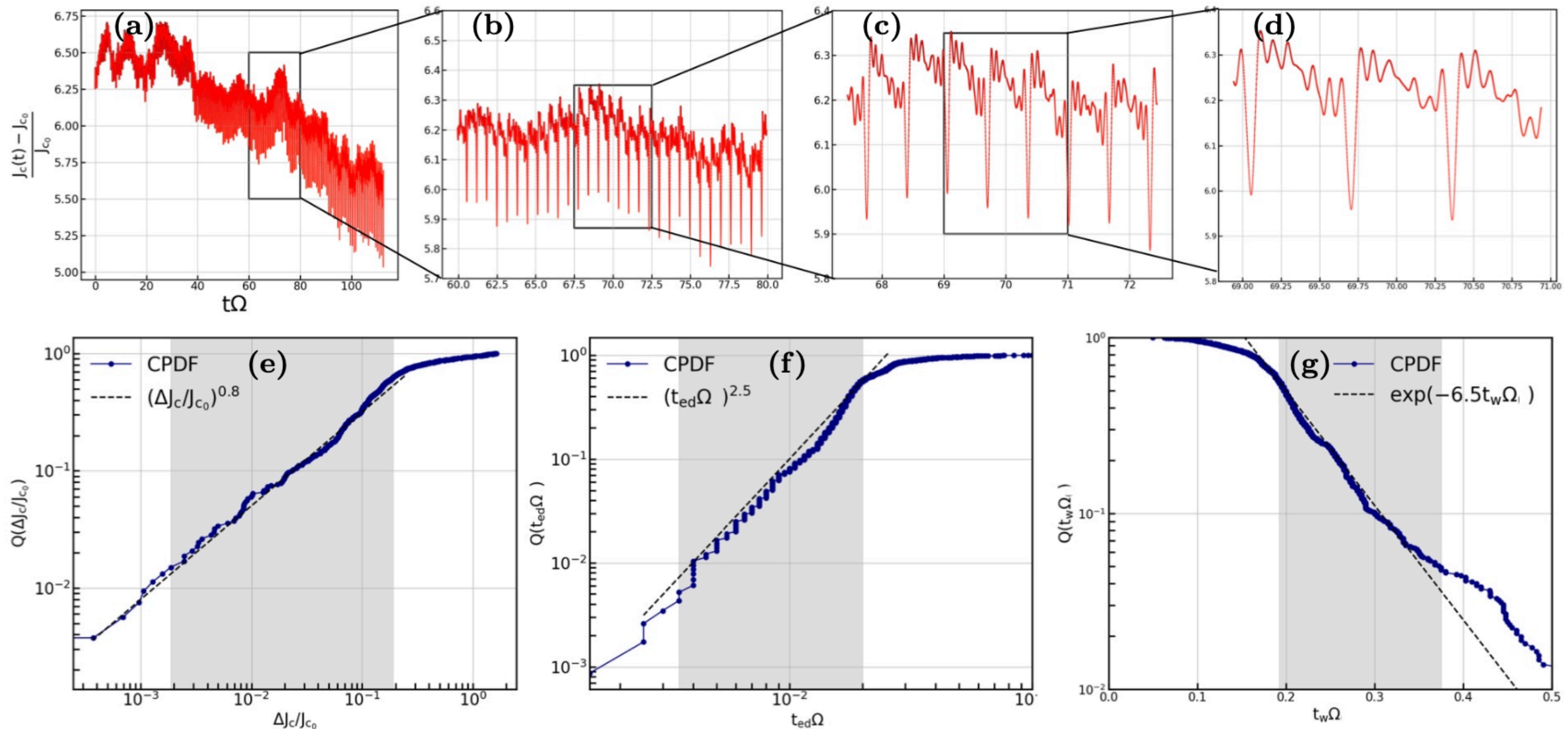


FIG. 13. **(a)** Time series of the crust angular momentum $(J_c - J_{c_0})/J_{c_0}$. **(b)**, **(c)**, and **(d)** are the zoomed versions of the rectangular regions shown in the preceding plots. Log-Log plots of **(e)** the CPDF $Q(\Delta J_c/J_{c_0})$ of the event size and **(f)** the CPDF $Q(t_{\text{ed}}\Omega)$ of the event duration. **(g)** semilog plot of the CPDF $Q(t_w\Omega)$ of the waiting time. J_{c_0} and Ω are the initial angular momentum and initial angular velocity of the crust, respectively.

Conclusion

what was done

- all codes were made in Bangalore
- pseudospectral spectrally truncated GPPE and SGLPE
- this work is part of the thesis of 2 of R. Pandit's students: Sanjay Shukla and Akhilesh Kumar Verma
- the classical field description of finite-T effects works well for those self-gravitating rotating BEC
- those minimal models reproduce surprisingly well some statistical large-scale effects

Thank You!